

**DOT/FAA/AR-97/82**

Office of Aviation Research  
Washington, D.C. 20591

# **Assessment of an Advanced Containment System**

February 1999

Final Report

This document is available to the U.S. public  
through the National Technical Information  
Service (NTIS), Springfield, Virginia 22161.



U.S. Department of Transportation  
**Federal Aviation Administration**

## **NOTICE**

This document is disseminated under the sponsorship of the U.S. Department of Transportation in the interest of information exchange. The United States Government assumes no liability for the contents or use thereof. The United States Government does not endorse products or manufacturers. Trade or manufacturer's names appear herein solely because they are considered essential to the objective of this report.

This report is available at the Federal Aviation Administration William J. Hughes Technical Center's Full-Text Technical Reports page: [www.tc.faa.gov/its/act141/reportpage.html](http://www.tc.faa.gov/its/act141/reportpage.html) in Adobe Acrobat portable document format (PDF).

1. Report No. DOT/FAA/AR-97/82		2. Government Accession No.		3. Recipient's Catalog No.	
4. Title and Subtitle ASSESSMENT OF AN ADVANCED CONTAINMENT SYSTEM				5. Report Date February 1999	
				6. Performing Organization Code	
7. Author(s) Kenneth L. Presley				8. Performing Organization Report No. AST Report No. R8008-1	
9. Performing Organization Name and Address  Advanced Structures Technology, Inc. 2851 S. 44th Street, Ste #4 Phoenix, AZ 85040				10. Work Unit No. (TRAIS)	
				11. Contract or Grant No. DTRS-57-90-C-00026	
12. Sponsoring Agency Name and Address  U.S. Department of Transportation Federal Aviation Administration Office of Aviation Research Washington, DC 20591				13. Type of Report and Period Covered Final Report	
				14. Sponsoring Agency Code ANE-100 and ANM-100	
15. Supplementary Notes The Federal Aviation Administration William J. Hughes Technical Center COTR is Bruce Fenton.					
16. Abstract  An advanced turbine engine fan blade containment system using ceramic tiles on a polymer fiber backing ring is proposed. The proposed ceramic/polymer-fiber system has proven more weight effective than monolithic metallic or polymer materials for stopping penetration of ballistic munitions projectiles. It was expected that this technology, originally developed for aircraft armor systems, could decrease containment system weights while still providing the same degree of protection as existing systems. This technology would allow for the design of higher thrust-to-weight engines and be used either for new designs or for retrofit application for existing engines. This program concluded that ceramic liners do not improve the performance of metal or composite containment structures for turbine engine uncontainment when evaluated in terms of contained energy per unit weight.					
17. Key Words Turbine engine containment, Propulsion systems, Composites and lightweight materials			18. Distribution Statement This document is available to the public through the National Technical Information Service (NTIS), Springfield, Virginia 22161.		
19. Security Classif. (of this report) Unclassified		20. Security Classif. (of this page) Unclassified		21. No. of Pages 23	22. Price

## PREFACE

This is the final report under contract number DTRS-57-90-C-00026, "Development of an Advanced Containment System." The program was a Phase II SBIR follow-on to the Phase I SBIR program analytical study conducted under contract number DTRS-57-88-C-00117. The results of the Phase I program were reported in the Federal Aviation Administration (FAA) report number DOT/FAA/CT-89/20, August 1989, "Development of an Advanced Fan Blade Containment System."

The reported work is related to a change proposed to 14 Code of Federal Regulations (CFR) Part 29 in October of 1989 in which rotor burst protection would be required for new design rotorcraft. The research reported herein was driven by the need to assess technologies which might minimize the adverse impact of such a rule change. The program was thus focused on containment systems for protection against turbine disk failures in small turboshaft engines operating primarily on rotary wing aircraft.

Bruce Fenton at the FAA William J. Hughes Technical Center at the Atlantic City International Airport, New Jersey, was the program technical monitor. Spin pit testing was conducted at the spin pit facility at the Naval Air Warfare Center in Trenton, New Jersey. Simula Inc. of Phoenix, AZ, was a major subcontractor for the design and fabrication of the aramid composite rings which were tested in this program.

## TABLE OF CONTENTS

	Page
EXECUTIVE SUMMARY	vii
1. INTRODUCTION	1
2. BACKGROUND	2
3. METAL RING PROGRAM	4
3.1 Test Article Design Method	4
3.2 Test Article Design Results	7
3.3 Test Results	9
3.4 Discussion	10
4. COMPOSITE RING PROGRAM	11
4.1 Ring Design and Construction	11
4.2 Test Results and Analysis	12
4.3 Discussion	15
5. CONCLUSION	15
6. REFERENCES	15

## LIST OF FIGURES

Figure		Page
1	Containment System Concept	1
2	Design Threat for This Study	2
3	Stage 1 Failure Mode: Perforation	3
4	Stage 2 Containment Characteristics	3
5	Florence's Observation on Projectile/Armor Interaction	4
6	Incorporation of Effect of Ceramic Into Method of Hagg and Sankey	6
7	Predicted Design Characteristics	9

## LIST OF TABLES

Table		Page
1	Design Results Summary	9
2	Test Results Summary	10
3	Construction and Design of Composite and Ceramic-Composite Containment Rings	12
4	Test Conditions and Results for Ceramic-Composite Containment Rings	13
5	Threshold Performance Comparison	15

## EXECUTIVE SUMMARY

The objective of this program was to evaluate the potential benefit of adding ceramic liners to turbine engine containment structures. Military ballistic programs have shown that ceramics can alter the ballistic projectile and increase the effective impact area to provide significant benefit. Turbine engine failures generate slower moving, odd-shaped debris. This effort added ceramic liners to metal and composite containment rings to evaluate the energy absorbed as a function of component weight.

For metal and composite containment structures, the container energy per unit weight was not improved by adding ceramic liners.

## 1. INTRODUCTION.

The objective of the program was to determine the potential weight savings of using a hard ceramic liner on the internal diameter of containment rings for disc burst containment applications. Figure 1 shows the containment system concept. Both metal and aramid composite rings with ceramic liners were investigated. A factor in considering ceramic-lined metal rings was their possible use in the hot section of the engine.

The use of a ceramic facing with composite and metal backings has been shown to be more weight efficient than monolithic composite or metal armor systems in ballistic armor applications. This weight efficiency in armor applications was the basis for investigating the technology applied to disc burst applications. Analytical studies performed under Phase I of this program, reported in reference 1, indicated that ceramic armor systems would be weight efficient in containing failed turbine engine rotor blades.

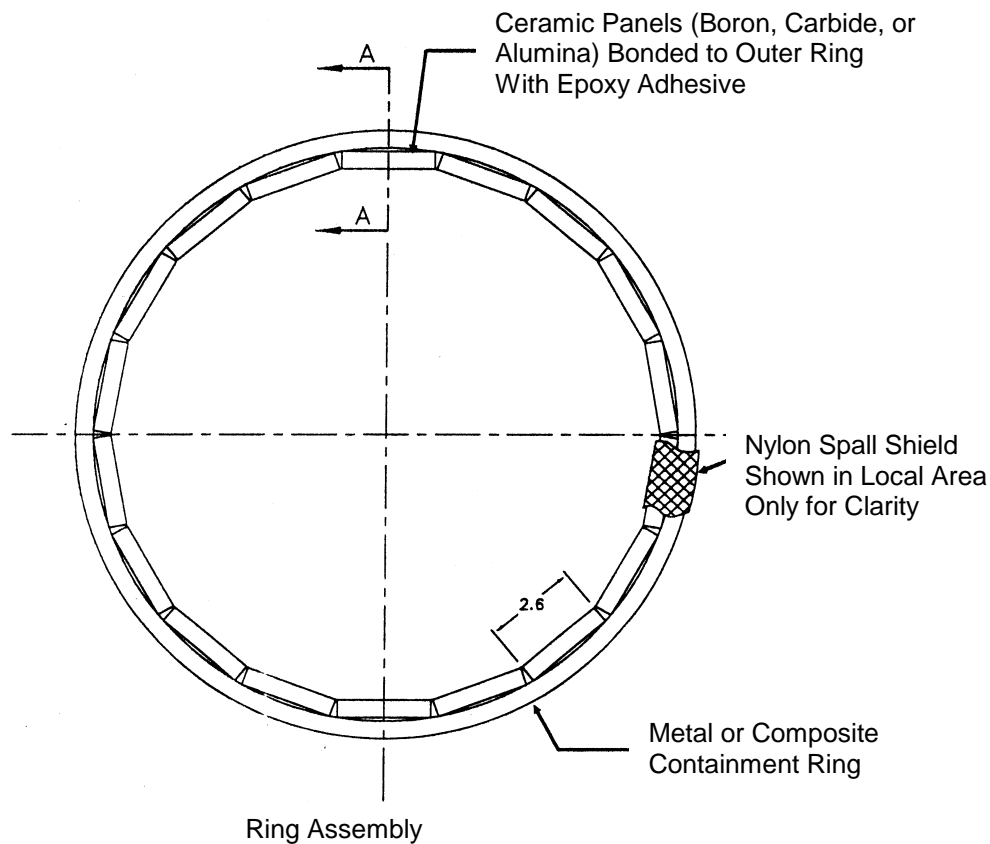


FIGURE 1. CONTAINMENT SYSTEM CONCEPT

This program included an analytical effort to design test articles and a series of spin pit tests involving 3-piece disc bursts of T-53 turbine wheels at the Naval Air Propulsion Center's (NAPC) spin pit test facility. The ballistic characteristics for the T-53 wheel burst are defined in figure 2. Spin pit test procedures and apparatus were as described in reference 2.

Monolithic metal and aramid composite rings were tested to determine the minimum weight for containment for the monolithic rings. Then, ceramic-faced rings of the same and lighter weight were tested to assess the weight saving potential from adding a layer of ceramic.

T-53 Turbine Disc Tri-Hub Burst  
Burst Speed - 20,000 RPM  
Preburst Kinetic Energy - 1,000,000 in-lb.  
Blade-Tip Diameter - 13.47 in.  
Disk Rim Diameter - 8.4 in.  
Disk Rim Width - 1.0 in.  
Total Wheel Mass - 10.8 lb.  
Single-Fragment Mass - 3.6 lb.  
Fragment Centroid Radius - 3.239 in.

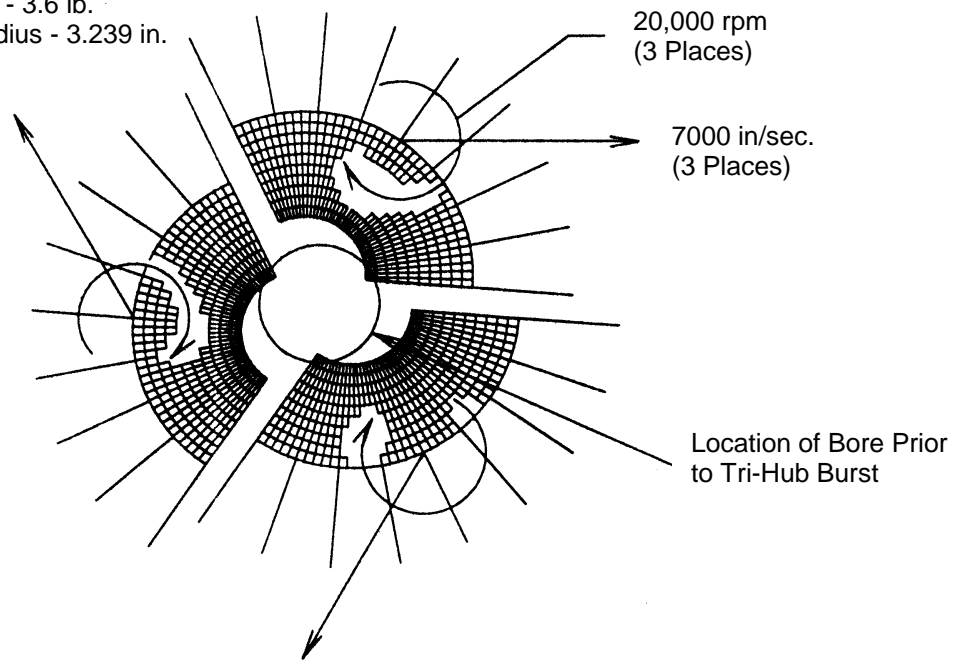


FIGURE 2. DESIGN THREAT FOR THIS STUDY

## 2. BACKGROUND.

Containment of a disk burst requires that the containment system prevent perforation of the containment ring and also absorb the substantial translational kinetic energy of the large disk fragments. The mechanism by which the energy is absorbed is dependent on the characteristics of the fragment and of the containment system. This study was confined to ring type structures intended to fully contain all disc fragments within the confines of the engine as opposed to other containment concepts such as flat panels strategically located to protect particular areas of an aircraft.

A.C. Hagg and G.O. Sankey observed the mechanisms by which a ductile metal ring defeats a rotor disc fragment in their disc burst containment testing [3]. The general description is also applicable to composite rings. The energy of the fragment is dissipated in two sequential stages. Noncontainment in the two distinct stages results in two different failure modes.

The first stage is the initial inelastic impact of the fragment with the ring. An amount of energy is dissipated in compressive and shear strain in the localized region of the impact of the fragment on the ring. Noncontainment in this stage results in the perforation of the ring in a local area. In metal rings, the disc fragment punches a hole in the ring carrying with it a shear plug as shown in figure 3. For composite rings, this first stage is characterized by tearing and cutting of the fibers in the local area of impact by the rotating fragment. Failure in this stage in the composite ring also results in perforation.

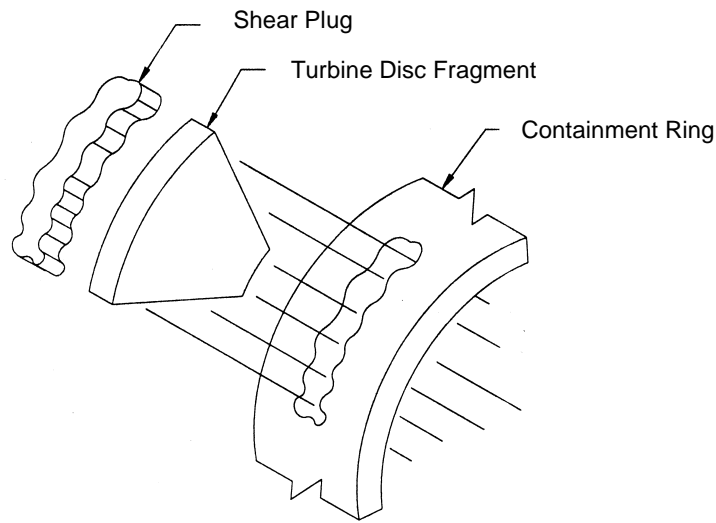


FIGURE 3. STAGE 1 FAILURE MODE: PERFORATION

If the ring contains in stage 1, then in stage 2 the remaining fragment energy is dissipated by inelastic elongation of the ring and bending as the ring is deformed into a lobed shape driven by the number of disc fragments. Noncontainment in this stage results from a tensile failure of the ring as shown in figure 4.

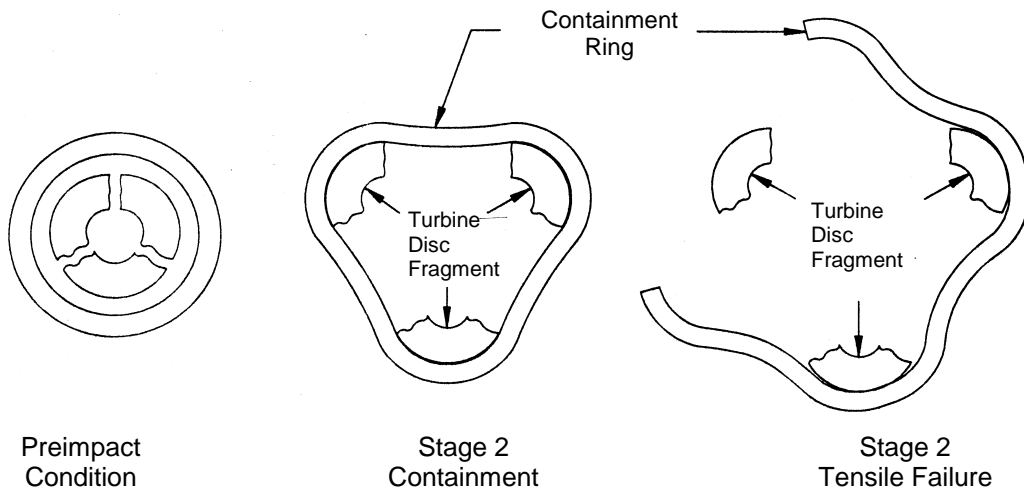


FIGURE 4. STAGE 2 CONTAINMENT CHARACTERISTICS

Florence [4] describes the mechanism by which a ceramic composite armor system defeats a high-velocity bullet type threat. This description is illustrated in figure 5. The hard ceramic facing in the armor system blunts the projectile and breaks up the hard armor piercing core. The impact forms a fracture conoid of finely pulverized ceramic which spreads the momentum of the impact over the area of the backing at the base of the conoid allowing a larger volume of that material to be involved in inelastic absorption of the projectile energy. The backing responds to the impact in a diaphragm-like manner. With fiber backings, energy is absorbed in delamination and in stretching and breaking of the fibers. With ductile metal backings, the energy is absorbed in inelastic deformation of the backing.

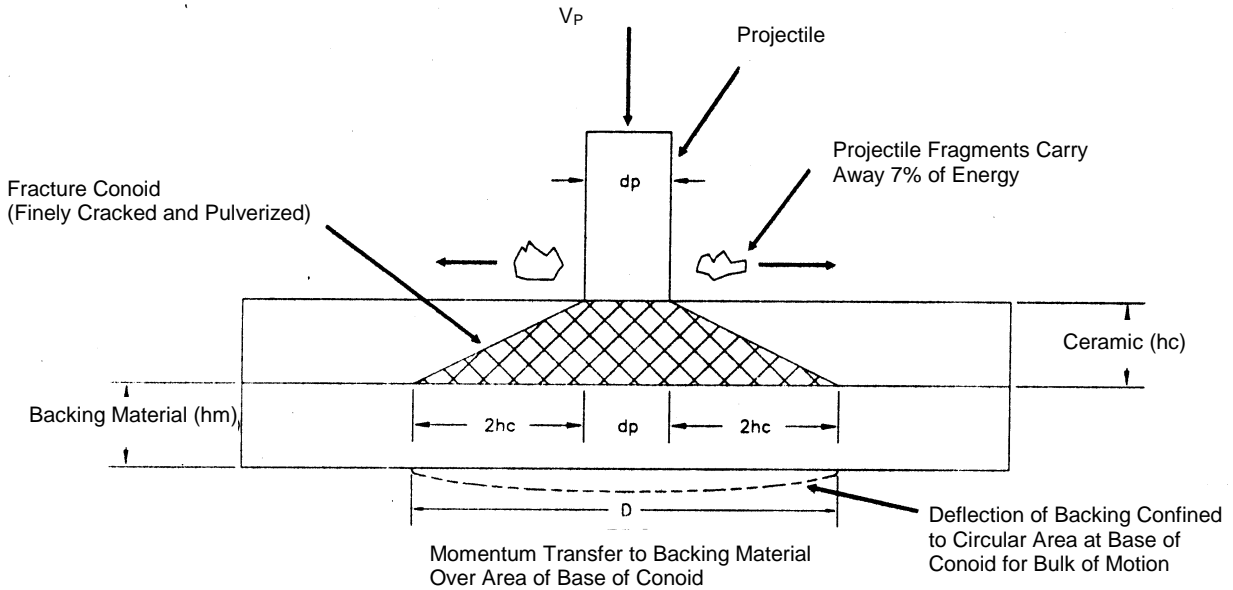


FIGURE 5. FLORENCE'S OBSERVATION ON PROJECTILE/ARMOR INTERACTION

### 3. METAL RING PROGRAM.

#### 3.1 TEST ARTICLE DESIGN METHOD.

Test articles were designed using an integration of the methods of Hagg and Sankey [3] (H&S hereafter) on the design of ductile metal containment rings with the approach of Florence [4] on the design of ceramic armor systems.

The following equations from H&S modified as discussed below define the containment criteria.

$$\text{Stage 1 Energy} \quad \Delta E_1 = 1/2 M_1 V_1^2 \left( 1 - \frac{M_1}{(M_1 + M_2)} \right) \quad (1)$$

$$\text{Stage 1 Containment criteria} \quad \Delta E_1 \leq A \bar{E} \quad \sigma_c \quad d + \kappa_d P T^2 + \mathcal{E}_\theta \sigma_f \quad (2)$$

$$\text{Stage 2 Energy} \quad \Delta E_2 = 1/2 M_1 V_1^2 \left( \frac{M_1}{(M_1 + M_2)} \right) \quad (3)$$

$$\text{Stage 2 Containment criteria} \quad \Delta E_2 \leq Q \sigma_d \varepsilon_t \quad (4)$$

$\Delta E_1$	Stage 1 energy
$\Delta E_2$	Stage 2 energy
$M_1$	Disc fragment mass
$M_2$	Target mass
$V_1$	Disc fragment translational velocity
$A$	Contact area of disc fragment on ring
$T$	Ring thickness
$\varepsilon_c$	Shear plug compression strain
$\varepsilon_t$	Average tensile strain in $Q$
$\sigma_d$	Dynamic flow stress
$K$	Empirical coefficient ( $K\tau_d = 0.27\sigma_d$ from H&S)
$\tau_d$	Dynamic shear stress
$P$	Shear plug perimeter
$V$	Volume of ceramic fracture conoid
$\varepsilon_\theta$	Equivalent ceramic strain
$\sigma_f$	Equivalent ceramic plastic flow stress
$h$	Disc fragment rim width
$t_c$	Ceramic thickness
$Arc$	Disc fragment arc length contacting ring
$a$	Plastic hinge length
$k$	Radius of gyration about plastic hinge
$L$	Ring width
$Q$	Active volume subjected to tensile strain
$\rho_c$	Ceramic density
$\rho_m$	Metal ring density

H&S's stage 1 containment prediction is based on a calculation of the energy dissipated in the initial impact compared to the energy required to perforate the ring. The perforation energy involves the inelastic compression of a shear plug and the energy to shear the plug out of the ring. The challenge in this study was to incorporate the effect of the ceramic into these energy calculations.

Several effects noted by Florence were incorporated into the H&S calculations based on a hypothesis that a fracture conoid similar to that observed in bullet impact would be formed in a turbine disc impact with a ceramic-faced ductile metal ring. Figure 6 shows the assumed disc impact mechanics. The dimensions of the ceramic fracture conoid were taken from reference 4.

The first adjustment made to the H&S prediction method was to add the mass of the conoid to the target mass,  $M_2$ . From equation 1, it can be seen that this tends to increase the energy,  $\Delta E_1$ , in equation 1.

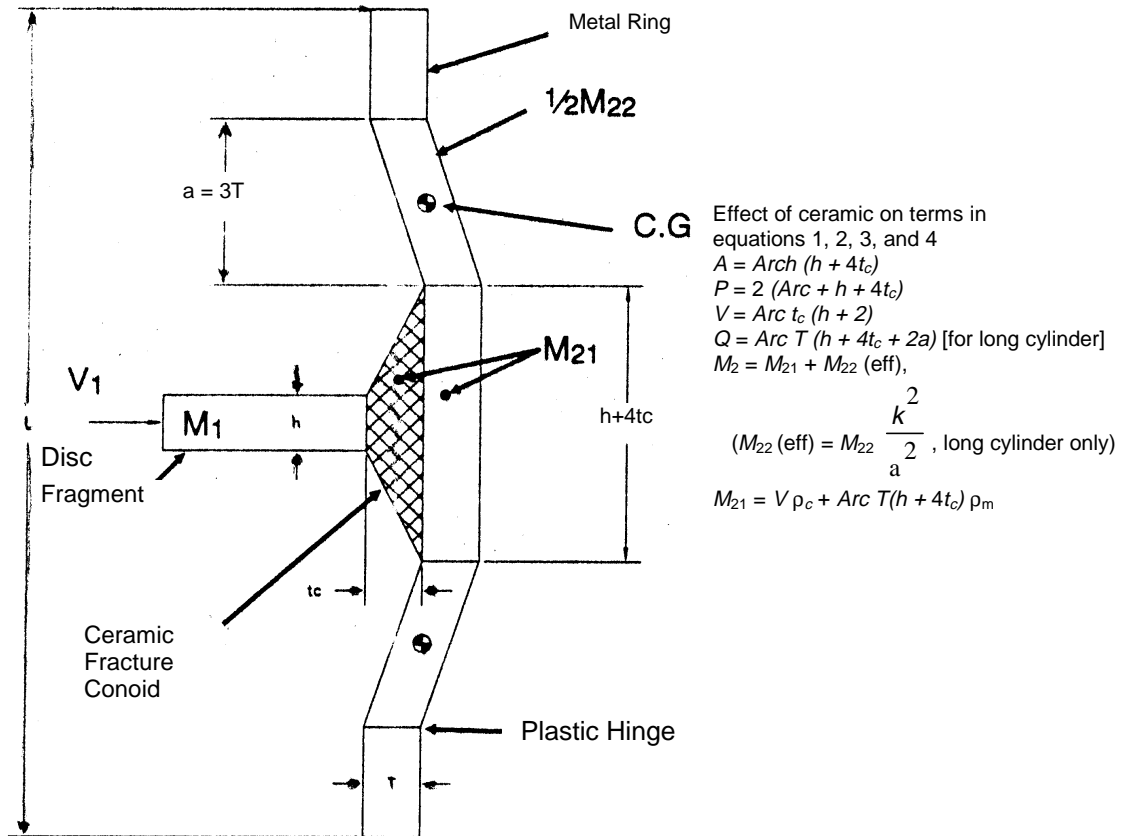


FIGURE 6. INCORPORATION OF EFFECT OF CERAMIC INTO METHOD OF HAGG AND SANKEY

As for armor systems, the ceramic conoid was expected to spread the disc impact momentum to a larger area of the ring than would be experienced with direct impact of the disc fragment on the ring. The second adjustment on the H&S prediction method was to incorporate the momentum spreading effect by adjusting the size of the shear plug to equal the area at the base of the fracture conoid. Increasing the area of the shear plug increases the compressive area of the shear plug,  $A$ , and the shear perimeter,  $P$ , in equation 2, thus increasing the energy absorption capability of the ring.

Since the H&S method is energy based, a third adjustment made to the H&S prediction method was to estimate and add in the energy involved in the initial impact with the ceramic in which the fracture conoid is formed. This energy is analogous to and additive to the compressive energy involved in inelastic compression of the shear plug. It was estimated as described below.

The literature search of armor data did not reveal any method for predicting the energy involved in the formation of the fracture conoid. Florence's description of the ceramic in the fracture conoid as very finely pulverized led to a hypothesis that the energy involved is proportional to the volume of the fracture conoid. This is similar to the energy absorption of ductile materials where the energy involved in plastic deformation, the integral under the stress strain curve, is proportional to the volume of strained material. Applying this hypothesis to ceramics requires the estimation of an equivalent plastic flow stress and strain, as discussed below.

Test data reported in reference 4 showed that a 0.34-in.-thick ceramic panel with a 0.25-in.-thick armor backing experienced a 0.272-cubic in. fracture conoid when impacted by a 30 caliber bullet with 2780 ft-lb of energy. Florence observed that in the initial impact the nose of the projectile shattered with the pieces carrying away approximately 7% of the projectile energy. To develop a design method, it was assumed that for the particular 2780 ft-lb bullet test described above the energy involved in forming the fracture conoid was equal to the 7% of projectile energy carried away by the shattering of the bullet nose. Using the flexural strength of ceramic as the equivalent plastic flow stress, an equivalent strain can be calculated to give an equivalent strain energy equal to 7% of the projectile energy. The flexural strength was chosen based on Florence's description of fractures in the ceramic being the result of tensile stresses that follow the compressive stress wave front which is analogous to a flexural situation.

For stage 2,  $Q$  in equation 4 is adjusted depending on whether the containment ring acts as a short cylinder or long cylinder. A long cylinder is characterized as having a length greater than the width of the disc fragment plus six times the ring thickness and vice versa for the short cylinder. For short cylinders, the entire ring is considered active volume. For long cylinders, only a localized region around the impact area is considered active. This volume has a width equal to the width of the disc fragment plus three times the ring thickness, a length equal to the arc length of the disc fragment, and a thickness equal to the ring thickness.

Since the ceramic layer is not thought to contribute in any way to the stage 2 energy absorption, all stage 2 energy was accounted for in the metal ring deformation. The only adjustment associated with the ceramic was to use the width of the fracture conoid as the width of the disc fragment in calculating  $Q$  for long cylinders.

### 3.2 TEST ARTICLE DESIGN RESULTS.

The basic ring configuration of figure 1 was selected early in the program based on its simplicity and ease of fabrication while answering the basic question of the potential benefit of a layer of ceramic on a metal ring. Boron carbide was selected as the ceramic of choice due to its low density and success in armor applications. Two design parameters were left to be selected, the ring geometry (diameter and length) and the metal ring material.

For a given ring geometry and material, the minimum metal thickness was calculated to predict containment without ceramic and with a given ceramic thickness. Each set of calculations was made assuming either short- or long-cylinder behavior with it being a post run judgment which assumption, short or long, was most applicable.

The following material properties were used for the test article design. The following design properties were derived from H&S.

$$\sigma_d = 1.25 \times \text{material ultimate tensile strength}$$

$$\varepsilon_t = 0.25 \times \text{material strain at tensile failure}$$

$$\varepsilon_c = 0.7 \varepsilon_t$$

$$K\tau_d = 0.27\sigma_d$$

The following properties were used for boron carbide ceramic.

$$\varepsilon_c = 17\%$$

$$\sigma_f = 50 \text{ ksi}$$

Preliminary parametric analyses were conducted in which three metal ring materials were looked at, Inconel 625, Titanium 6AL-4V, and a generic 300 series stainless steel. Two geometric parameters were investigated, ring lengths of 2, 3, 4, and 5 inches and ring diameters of 16 and 24 inches.

Several general results were noted. The ceramic layer was shown to offer a weight benefit with both the Inconel 625 and the generic 300 series stainless steel but not with the titanium. Shorter rings were shown to be lighter than longer rings and the ceramic showed increasing weight benefit with increasing ring length.

The 16-inch ring diameter was selected based on its consistency with an extensive program at the Federal Aviation Administration (FAA) and NAPC involving 15-inch rings of various materials and also the analytical result showing the smaller the ring diameter the lower the total weight. The 16-inch diameter allows room for the ceramic layer within the ring. The predicted weight benefit of the ceramic increased with the length of the ring. This, combined with a desire to have as low a total weight ring as possible, suggested selection of the shortest ring which showed a substantial predicted weight benefit. Thus, the 4.0-inch ring length was selected. The analytical prediction did not show any weight benefit of ceramic with titanium so it was eliminated. A weight benefit was predicted for Inconel 625 and the generic 300 series stainless steel. The 300 series stainless steel was selected based on cost. Figure 7 shows the predicted 300 series stainless steel ring thickness and weight as a function of the ceramic thickness. Table 1 summarizes these results.

Cres 321 stainless steel was selected as the specific ring material based on its combination of relatively high strength and high ductility amongst the 300 series stainless steels. Flash butt welded ring construction per AMS 7490 was selected based on the ability to have good strength and ductility in the weld area. All rings were solution heat treated and subjected to a complete x ray. Test properties for the parent material were 78,900 psi tensile strength with 52.9% elongation and 74,000 psi tensile strength with 37.1% elongation for the weld area.

The boron carbide ceramic tiles were bonded to the metal ring with an epoxy. A nylon spall shield was wrapped over the tiles and bonded in place with a contact adhesive.

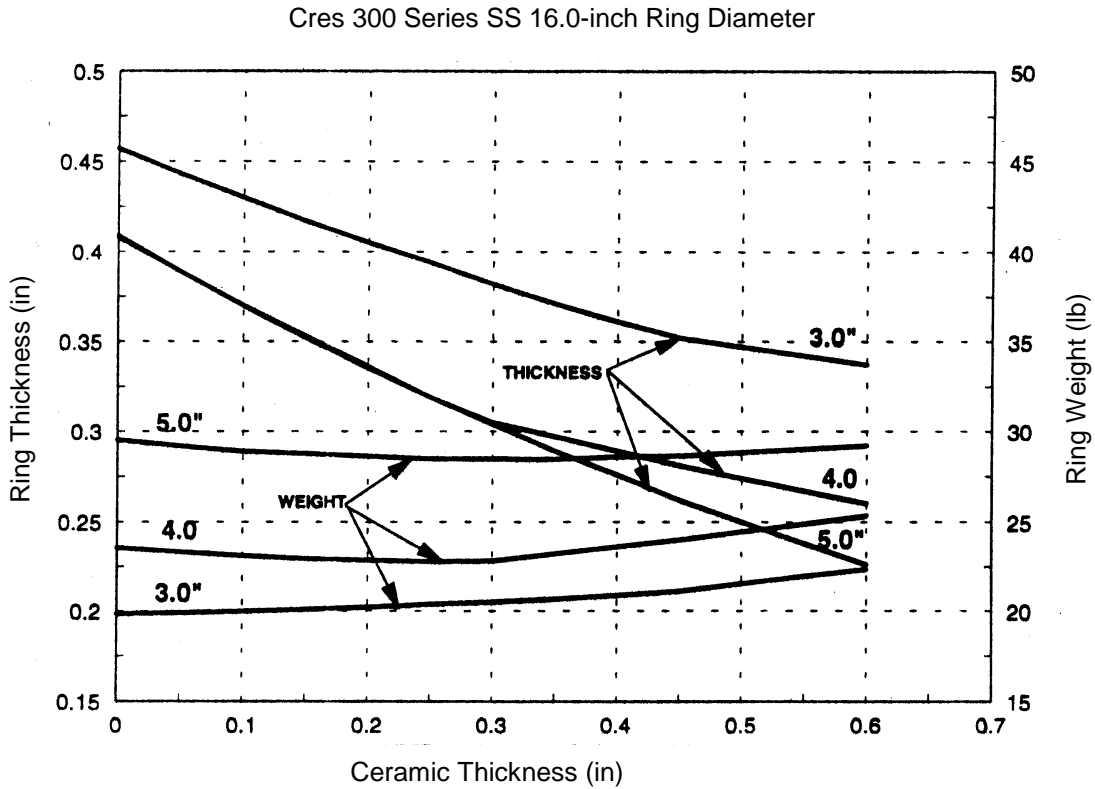


FIGURE 7. PREDICTED DESIGN CHARACTERISTICS

TABLE 1. DESIGN RESULTS SUMMARY

	Length	Ring Thickness	Ceramic Thickness	Total Weight	Weight Benefit
300 Series Stainless Steel Shell (Long Cylinder Behavior 16.0-in. Diameter)	3.0	0.457	0.0	19.85	0.0 lb
	4.0	0.408	0.0	23.55	0.8 lb
		0.319	0.25	22.77	
	5.0	0.409	0.0	29.52	1.1 lb
			0.35	28.42	

### 3.3 TEST RESULTS.

Table 2 summarizes the test results. Six tests were run over a period of 7 months. All the tests were considered valid tests with all burst speeds within 6% of the target burst speed of 19,843 rpm and all impacts being well centered on the containment rings.

Four monolithic metal containment rings and two ceramic-lined metal containment rings were tested. Three of the monolithic rings and one of the ceramic-lined rings resulted in containment. One of the monolithic rings and one of the ceramic-lined rings resulted in noncontainment.

Substantial local tearing and scuffing on the inner diameter of the rings was noted on both the monolithic and ceramic-lined rings. The local tearing and scuffing on the ceramic-lined rings was noticeably less than on the monolithic rings.

TABLE 2. TEST RESULTS SUMMARY

Test Date	Ring <sup>1</sup> Thickness (in)	Ceramic <sup>3</sup> (in)	Total Ring Weight (W) (lb)	Metal Weight (Wm) (lb)	Ceramic <sup>2</sup> Weight (lb)	Burst Speed (rpm)	Burst Energy (E) (in-lb)	E/W (in-lb/lb)	E/Wm (in-lb/lb)	Result	Failure Mode
08/09/91	0.450	0.00	26.00	26.00	0	20,280	956,733	36,797	36,797	Contained	—
08/20/91	0.378	0.00	21.75	21.75	0	20,150	944,506	43,425	43,425	Contained	—
08/23/91	0.307	0.00	17.75	17.75	0	19,600	893,649	50,346	50,346	Uncontained	Tensile
03/02/92	0.343	0.00	20.25	20.25	0	20,692	996,001	49,185	49,185	Contained	—
03/05/92	0.288	0.275	21.62	16.08	5.54	20,240	952,962	44,078	59,264	Contained	—
03/11/92	0.251	0.275	19.84	14.28	5.56	21,100	1,035,666	52,439	72,526	Uncontained	Tensile

1. Tolerance band 0.265-0.285 in  
2. Includes ceramic tile, epoxy, nylon spall shield  
3. All rings had an internal diameter of 15.50-15.56 in. with a length of 3.97-4.03 in.

All the rings showed a substantial local deformation in the disc impact area. The local deformation was very similar from ring to ring with test number 6 showing the most severe local deformation. No significant difference was noted in the shape or extent of the local deformation between the ceramic-lined and monolithic rings.

Both rings which did not contain failed in tension, the Stage 2 failure mode of H&S. In both cases the failure location was in the disc impact area where the local deformation associated with the disc impact was additive to the overall bending deformation associated with the ring being deformed into a three-lobed shape.

The ceramic tiles were pulverized into a large number of relatively small pieces with the largest being roughly 1/2" on a side. Only very small pieces of ceramic remained bonded to the metal ring. In the high-speed photographs, it was observed that a small quantity of dust was formed when the turbine blade tips contacted the ceramic tiles on the inner diameter of the ring. A small dust cloud was formed obscuring the tips of the blades. This dust cloud grew as the impact process proceeded, ultimately obscuring most of the turbine disc pieces and the containment ring.

### 3.4 DISCUSSION.

Four tests were key in reaching conclusions concerning the objective of the research program, tests 3 and 4 of the monolithic rings and tests 5 and 6 of the ceramic-lined rings.

From tests 3 and 4, it was determined that the threshold containment weight for the T-53 turbine disc burst is 20 lbs. This is based on both tests having similar energy-to-weight ratios, test 3 failing to contain at a little over 50,000 in-lb/lb and test 4 containing at a little under 50,000 in-lb/lb.

Test 5 of the ceramic-lined ring showed a containment at an energy-to-weight ratio of 44,078 in-lb/lb and a total weight of 21.62 lb while test 6 showed a failure to contain at an energy-to-weight ratio of 52,439 in-lb/lb with a total weight of 19.84 lb. The 52,439 in-lb/lb is less than 5% above the threshold energy-to-weight ratio for the monolithic ring.

Based on these results, no meaningful weight benefit can be expected from the ceramic lining of metal rings with similar configuration and materials to those tested in this program.

While ceramic-based systems have proven themselves in armor applications, it is apparent that there are substantial differences in the disc burst containment application which may be the reason that a meaningful weight benefit was not found. From the high-speed photographs, it can be seen that the turbine blades begin the process of breaking up the ceramic before the high-momentum disc pieces reach the ring. The benefit of the ceramic is predicated on its ability to spread the impact momentum over a larger area of the ring than would be the case with a direct impact on the ring. With the ceramic already broken up at the time of disc impact, this momentum spreading effect is greatly reduced or eliminated. This lack of momentum spreading is generally confirmed by the size and shape of the local deformation in the impact area being essentially the same with and without the ceramic.

#### 4. COMPOSITE RING PROGRAM.

Composites are most often not hard enough to perform well as monolithic containment ring materials. Compared to conventional containment ring materials, like steel and titanium, composites have little or no ability to blunt the edges of fragments which impact them. The resulting fragments can have very sharp edges which easily cut the composite fibers, significantly reducing their containment capability. Prior research has shown that using a liner of a harder material can improve the efficiency of the composite containment rings. The purpose of this program was to evaluate the performance of ceramic liners for composite containment rings.

#### 4.1 RING DESIGN AND CONSTRUCTION.

A baseline (threshold containment) monolithic composite containment ring was developed from existing data and experimental results. This ring was used as a reference for comparison with ceramic-composite rings. All rings fabricated under this program were 4 in. wide.

A total of nine rings were fabricated for this program as shown in table 3. All rings used aramid fibers and a modified epoxy resin for the composite part of the rings. Aramid fibers were selected because of their lightweight, thermal stability, and postimpact integrity. The epoxy resin was selected for its compatibility with the aramid and its flexibility in processing. The ceramic selected for the hard face on the rings was boron carbide (B4C). This material was selected for its low density and high hardness and toughness.

TABLE 3. CONSTRUCTION AND DESIGN OF COMPOSITE AND CERAMIC-COMPOSITE CONTAINMENT RINGS

Ring No.	Weight (lb)	Number of Plies	Areal Density (lb/ft <sup>2</sup> )	Comments
1	9.70	18	6.494	Baseline configuration
2	9.34	~19	6.225	Lower fiber angle, stitched down middle
3	11.0	22-24	7.173	Stretched on mandrel, low fiber angle
4	21.7	38	13.343	Tapered lay-up, low fiber angle, some buckling in laminate due to cure process
5	16.04	32	10.338	Tapered lay-up, low fiber angle
6	13.29	28	8.682	Very good ring, tapered lay-up, low fiber angle
7	12.08	26	7.958	Low fiber angle, fairly consistent ring
7C	5.68/6.90*	11	3.950/4.26*	Thinnest ring fabricated, made over a core to account for ceramic liner, very consistent thickness, used ~0.5 lb of toughened epoxy to bond tiles on, tile width was ~2.5 inches, height was ~4.0 inches
8	11.31	22	7.557	Low fiber angle, some fiber wash
NAPC 1	32	73	10.844	Aramid/phenolic ring, unknown construction
NAPC 25	22.50	54	7.819	Aramid/phenolic ring, unknown construction
*weight or areal density of composite/ceramic				

The construction of the rings was optimized in an iterative fashion. After each ring was tested, the residue was carefully examined to determine the failure mode. The specific energy absorption was calculated and compared to the other tests. Based on the findings, the next ring was fabricated with either more or less material to attempt to optimize the weight for the design impact energy.

For the ceramic-composite ring, the design (specifically the ceramic-to-composite ratio) was selected based on ballistic testing of armor samples and availability of material. From ballistic testing, it was found that ceramic that was too thin (less than 0.15 inch) would not perform well in an armor system and that ceramic that was too thick (over 0.50 inch) would weigh too much for the benefit it provided. The ceramic thickness selected for use in the containment ring was 0.30 inch. This was the thinnest available material that was over 0.15 inch thick. Ideally, the ceramic could have been thinner, which would have provided a higher weight fraction of composite backing, but the expense to obtain such material was found to be prohibitive considering the scope of the program. For this reason, the performance of the ceramic-composite ring cannot be considered to be optimized.

#### 4.2 TEST RESULTS AND ANALYSIS.

The results obtained from the spin pit testing are shown in table 4. The fifth column, the specific energy absorption, normalizes the impact energy by the areal density of each ring test. The

specific energy absorption is a measure of the efficiency for that particular ring design. Areal density was selected for normalization because it eliminates geometrical effects. Since the objective of this program was to evaluate materials or constructions rather than geometry, this method allows direct comparison of materials regardless of the geometry in which they were tested. This was particularly important in comparing the previously tested rings with those tested under this program.

TABLE 4. TEST CONDITIONS AND RESULTS FOR CERAMIC-COMPOSITE CONTAINMENT RINGS

Ring No.	Weight (lb)	Areal Density (lb/ft <sup>2</sup> )	Impact Energy (in-lb)	Specific Energy Absorption (in-lb/lb/ft <sup>2</sup> )	Contained? (Y/N)	Comments
1	9.70	6.494	1,025,000	157,838	N	
2	9.34	6.225	1,099,000	176,546	N	No outer ply failure, material twisted out of the way
3	11.0	7.173	977,000	136,205	N	Marginal failure, good tensile performance in outer plies
4	21.7	13.343	1,167,000	87,461	Y	No perforation, delamination throughout
5	16.04	10.338	1,060,000	102,534	Y	
6	13.29	8.682	1,160,000	133,610	Y	Very good containment
7	12.08	7.958	963,052	121,016	N	Possible perforation, no significant tensile failure
7C	5.68/6.90	3.950/4.26*	929,936*	113,268	N	Tensile failure in composite
8	11.31	7.557	N/A	N/A	N/A	Ring not tested
NAPC 1	32.00	10.844	968,000	89,265	Y	
NAPC 25	22.50	7.819	978,000	125,079	N	Partial containment
*weight or areal density of composite/ceramic						

Two rings tested previously at NAPC are shown at the end of the table; NAPC 1 and NAPC 25 are the most efficient aramid-reinforced systems previously tested. Though NAPC 25 did not fully contain the rotor burst, it was said to be very close to the critical value for ring efficiency (i.e., maximum specific energy absorption). The other data columns give absolute values for weight, areal density, and impact energy. The areal density has been calculated from known thickness and material density values and was used as a normalized value for weight. This eliminated any differences in specific energy absorption which might arise from differences in geometry.

The posttest condition of each ring was used as a gage to assess the type of failure which occurred. The first ring fabricated, Ring 1, was a very stiff ring which failed in a combined flexure/tension mode.

This indicated that the second ring needed to be less stiff to avoid the flexural failure mode. Thus, its overall weight is less, but the actual amount of fiber present is higher. In the test, the

second ring twisted out of the path of the disk segment; thus, not absorbing a significant amount of the impact energy.

The third ring was constructed with more plies of material to provide a higher overall tensile strength. This ring failed in pure tension which is the desirable failure mode. Though the failure appeared very marginal (almost contained), the fourth ring was fabricated significantly heavier to ensure containment. Rings 4 and 5 both contained the rotor burst without perforations or tensile failure in the outer plies.

The residue from Ring 6 showed a near-perfect containment, with the outer few layers remaining unbroken and the rotor segments lodged in the ring. The residue from Ring 7 showed a very different type of failure from the other rings. There were several large perforations of the ring at the points corresponding to the impact sites of the rotor segments. The outer plies did not fail in tension as they had with Rings 3 and 6.

Ring 7C showed similar performance to Ring 7, except that the perforations were somewhat larger and there was substantial ceramic residue in the perforations.

Table 5 lists the best performing rings from both sources. The highest passing (Ring 3) and lowest failing (Ring NAPC 1) (in terms of specific energy absorption) rings are listed. From these two data points an approximate value for the threshold specific energy absorption can be calculated. This is done by taking the average of these two values, as was done in the calculation of the V50 Protection Ballistic Limit for armor systems. From this, it can be seen that the average specific energy absorption for the rings fabricated by Simula is some 25 percent higher than that for the rings tested previously. Further testing is required to verify this number. It should be noted that Ring 7 has a specific energy absorption value lower than this calculated threshold value but failed to contain the disk. The same can be said for Ring 7C in table 4, a ceramic-faced composite ring.

One possible explanation for the failure of Ring 7 to contain the disk is that the overall thickness of the ring was so low. It is possible that the number of sacrificial layers, or those that are simply cut by the sharp fragments, is too high. Each of the rings which contained its rotor burst had from 16 to 20 layers through which the fragments cut before the tensile layers contained the energy of the now blunted fragment. Because of the lightweight of Ring 7, the total number of sacrificial layers is roughly equivalent to the total number of layers in the ring. Thus, there are few or no layers remaining to contain the fragments. This hypothesis is supported by the fact that there are several small (1 in<sup>2</sup>) perforations on the outer surface of the ring and no evidence of tensile failure in the plies.

For Ring 7C, which had a ceramic hard face to blunt the incoming fragments, there was not enough composite remaining at the given weight (12.5 lb in this case) to absorb the impact energy. There was predominant fiber cutting and perforation rather than tensile failure. As noted above, this ring used a thicker ceramic than desired that resulted in a low fiber weight. This suggests that further optimization of ceramic and composite thickness may yield a minor net weight improvement.

TABLE 5. THRESHOLD PERFORMANCE COMPARISON

Ring No.	-	Specific Energy Absorbed (in-lb/lb/ft <sup>2</sup> )	Normalized Specific Energy Absorbed	Contained? (Y/N)	Comments
6		133,610	1.0	Y	Simula's best construction
	average	134,907	1.0097	-	Average of high passing and failing
3		136,205	1.019	N	Lowest failing construction
7		121,016	0.9057	N	
	average	127,313	0.9529	-	Average of Rings 6 and 7, Ring 7 may not be a valid test because perforation by small fragments may have caused witness sheet perforation and a false failing result
NAPC 1		89,265	0.668	Y	Best performing ring from previous tests
	average	107,172	0.8021	-	Average of high passing and low failing ring values
NAPC 25		125,079	0.936	N	Lowest failing ring from previous tests

### 4.3 DISCUSSION.

Based on the test results shown above, the rings designed and fabricated by Simula show a slight improvement in critical specific energy absorption over those rings fabricated and tested previously by NAPC. Using the highest passing and lowest failing ring specific energy absorption values, this improvement is between 15.8 and 20.6 percent.

### 5. CONCLUSION.

The inclusion or addition of ceramic hard faces, at the relative ratios used in these tests, does not seem to improve the containment properties of the rings.

### 6. REFERENCES.

1. Lane, Alan D., "Development of an Advanced Fan Blade Containment System," DOT/FAA/CT-89/20, August 1989.
2. Salvino, J.R., Mangano, G.J., and DeLucia, R.A., Rotor Burst Protection: Design Guidelines for Containment, 79N27166 Issue 18, April 1979.
3. Hagg, A.C. and Sankey, G.O., "The Containment of Disk Bust Fragments by Cylindrical Shells," Journal of Engineering for Power, Trans. ASME, Paper No. 73-WA-Pwr-2.
4. Florence, A.L., "Interaction of Projectiles and Composite Armor," Part II, AMMRC CR 69-15, August 1969, NTIS AD 698543.